ADVANCED MATERIALS

Supporting Information

Magnetic Alignment for Plasmonic Control of Gold Nanorods Coated with Iron Oxide Nanoparticles

Mehedi H. Rizvi, Ruosong Wang, Jonas Schubert, William D. Crumpler, Christian Rossner, Amy L. Oldenburg, Andreas Fery, and Joseph B. Tracy*

Supporting Information

Magnetic Alignment for Plasmonic Control of Gold Nanorods Coated with Iron Oxide Nanoparticles

Mehedi H. Rizvi, Ruosong Wang, Jonas Schubert, William D. Crumpler, Christian Rossner, Amy L. Oldenburg, Andreas Fery, and Joseph B. Tracy*

Supporting Movies:

Movie S1 (.mp4 format). Polarization effect on MagGNRs using single 1-inch cube magnet

Movie S2 (.mp4 format). Polarization effect on MagGNRs using circular Halbach array

Movie S3 (.mp4 format). Polarization effect on MagGNRs using two arrays of five ¼-inch cube magnets

Movie S4 (.mp4 format). Polarization effect on MagGNRs using single array of five ¼-inch cube magnets

Movie S5 (.mp4 format). Polarization effect on MagGNRs using two arrays of two 10-mm cube magnets

Movie S6 (.mp4 format). Polarization effect on MagGNRs using two 10-mm cube magnets

Movie S7 (.mp4 format). Magnetic separation of MagGNRs using two arrays of two 10-mm cube magnets

Movie S8 (.mp4 format). Polarization effect on MagGNRs on a magnetic stir plate at 60 rpm

Movie S9 (.mp4 format). Oscillating colors of MagGNRs on a magnetic stir plate at speeds up to 1000 rpm

Model for Quantifying Magnetic Alignment and Estimating $U_{barrier}$

MagGNRs consist of a GNR core coated with highly monodisperse superparamagnetic NPs. Application of an external magnetic field **H** induces a magnetic moment **m** in each NP, which is assumed to be identical and parallel to **H**. We attribute magnetic alignment of MagGNRs to a potential energy difference $U_{barrier}$ between states with **m** aligned parallel versus perpendicular to the long axis of the GNR core (Equation 3). This approach mimics the treatment of GNRs in an optical trap, where the energy difference between parallel and perpendicular orientations relative to the polarization of an electromagnetic field is modeled.[1] The distinction here is that magnetic interactions are responsible for the trapping behavior.

We model the magnetic potential energy of a MagGNR, U_{MagGNR}, which we assume is dominated by magnetic dipole-dipole interactions between each pair of NPs on the MagGNR, i.e., U_{MagGNR} is the sum of the energies needed to bring each NP of moment **m** in one-by-one from infinity to its position on the MagGNR. This can be done by tabulating the dipole-dipole interaction energy U_{ij} between each new NP, j, with each existing NP, i, already placed:

$$U_{MagGNR} = \sum_{j} \sum_{i>j} U_{ij} \,, \tag{S1}$$

where the dipole-dipole interaction energy is:

$$U_{ij} = \frac{\mu_0}{4\pi \left|\mathbf{r}_{ij}\right|^3} \left(\vec{\mathbf{m}}_i \cdot \vec{\mathbf{m}}_j - 3\left(\vec{\mathbf{m}}_i \cdot \hat{\mathbf{r}}_{ij}\right)\left(\vec{\mathbf{m}}_j \cdot \hat{\mathbf{r}}_{ij}\right) \right), \tag{S2}$$

$\mathbf{r}_{ij}$ is the displacement vector between the centers of NPs i and j, and μ_0 is the permeability of free space. For superparamagnetic NPs, the time-averaged moment will point parallel to **H**, and its strength will depend on **H**. Given that the moments are identical, $\mathbf{m}_i = \mathbf{m}_j = \mathbf{m}$, the above simplifies to:

$$U_{ij} = \frac{\mu_0 \left|\mathbf{m}\right|^2}{4\pi \left|\mathbf{r}_{ij}\right|^3} \left(1 - 3\left(\hat{\mathbf{m}} \cdot \hat{\mathbf{r}}_{ij}\right)^2\right). \tag{S3}$$

We define γ_{ij} as the angle between $\mathbf{r}_{ij}$ and **H**, giving:

$$U_{ij}\left(\gamma_{ij}\right) = \frac{\mu_0 \left|\mathbf{m}\right|^2}{4\pi \left|\mathbf{r}_{ij}\right|^3} \left(1 - 3\cos^2 \gamma_{ij}\right). \tag{S4}$$

While Equation S4 provides important insight as it carries a negative cosine-squared dependency on angle, the same as the optical trap,[1] γ_{ij} are not generally the same as the angle θ between the long axis of the GNR and **H**, since the displacement between each pair of NPs is not generally along the GNR. Intuitively, we might expect that, when calculating the sum in Equation S1, the components of $\mathbf{r}_{ij}$ perpendicular to the long axis of the GNR would cancel out,

provided the NPs uniformly decorate the GNR. To analytically tabulate this effect, we rewrite Equation S3 in terms of θ and transform the coordinates from the lab frame (x,y,z) to the MagGNR frame (x',y',z') by rotation about the x-axis by ϕ and then about the z'-axis by θ. The diagram below depicts the new coordinate system translated along x' for clarity (i.e., the coordinate systems share the same origin, which is where the center of the MagGNR is located):
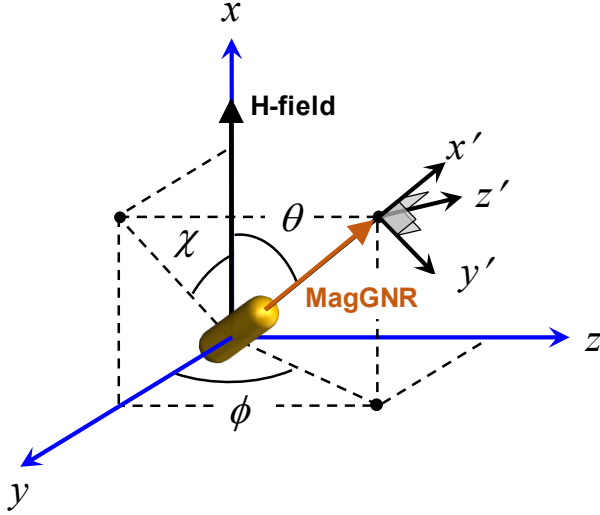
The components of $\mathbf{r}_{ij}$ along $\mathbf{H}$ can be written as:

$$\mathbf{r}_{ij} = \Delta x'_{ij}\hat{i}' + \Delta y'_{ij}\hat{j}' + \Delta z'_{ij}\hat{k}' , \tag{S5}$$

where $\Delta x'_{ij}$ and $\Delta y'_{ij}$ are the x'- and y'- displacement components between two NPs in the coordinate frame of the MagGNR (such that x' is along the long axis of the GNR). Using $\hat{\mathbf{m}} = \hat{i}$, we obtain:

$$\hat{\mathbf{m}} \cdot \hat{\mathbf{r}}_{ij} = \frac{\hat{i} \cdot \mathbf{r}_{ij}}{\left|\mathbf{r}_{ij}\right|} = \frac{\Delta x'_{ij}\cos\theta - \Delta y'_{ij}\sin\theta}{\left|\mathbf{r}_{ij}\right|} . \tag{S6}$$

There is no explicit $\Delta z'_{ij}$ dependence because the z'-axis is perpendicular to the x-axis. This is because we neglect a possible third rotation of the GNR coordinates about its long axis due to the assumed axisymmetry of the GNR. Substituting Equation S6 into Equation S3 and performing some algebraic manipulation gives:

$$U_{ij}(\theta) = \frac{\mu_0 \left|\mathbf{m}\right|^2}{4\pi \left|\mathbf{r}_{ij}\right|^3}\left(\left(1 - \frac{3\Delta y'^2_{ij}}{\left|\mathbf{r}_{ij}\right|^2}\right) - \left(\frac{3\left(\Delta x'^2_{ij} - \Delta y'^2_{ij}\right)\cos^2\theta}{\left|\mathbf{r}_{ij}\right|^2}\right) - \left(\frac{3\Delta x'_{ij}\Delta y'_{ij}\sin 2\theta}{\left|\mathbf{r}_{ij}\right|^2}\right)\right). \tag{S7}$$

Examining the three terms in parentheses, we see that the first term represents a constant offset independent of θ, which may be ignored because only potential energy differences are relevant to magnetic trapping (i.e., the potential energy offset can be arbitrarily set). The third term, being linear in both $\Delta x'_{ij}$ and $\Delta y'_{ij}$, is expected to sum to zero when applying Equation S1, since

3

the NPs are uniformly distributed about the MagGNR centered at $x' = y' = 0$. Therefore, only the second term is relevant for determining θ-dependence of U_{ij}. Since the MagGNR is prolate with its long axis along x', we expect that the $\Delta x'^2_{ij}$ terms will be larger than the $\Delta y'^2_{ij}$ terms when summed, such that the final result has the familiar negative cosine-squared relationship:

$$U_{MagGNR}(\theta) \sim -\cos^2\theta \frac{3\mu_0 |\mathbf{m}|^2}{4\pi |\mathbf{r}_{ij}|^5} \sum_j \sum_{i>j} \left(\Delta x'^2_{ij} - \Delta y'^2_{ij}\right).$$

$$= -n k_B T \cos^2\theta$$

(S8)

This shows explicitly how the trap depth n is related to the positions of the NPs and magnetic moments induced by the applied magnetic field. For example, the expression indicates how the greater the aspect ratio of the MagGNR, the more the $\Delta x'^2_{ij}$ terms dominate over the $\Delta y'^2_{ij}$ terms, thus increasing the trap depth.

Quantifying Magnetic Alignment from Optical Extinction Spectroscopy

In optical spectroscopy, we acquire extinction (also known as absorbance) A by measuring the optical intensity I incident and transmitted through a sample:

$$A = -\log_{10}\left(\frac{I_{transmitted}}{I_{incident}}\right),$$

$$\frac{I_{transmitted}}{I_{incident}} = e^{-C_{ext}Nz} = 10^{-A}$$

(S9)

where Beer's law is used to show that the extinction cross-section C_{ext} is proportional to A, via the number density of MagGNRs, N, and the optical path length through the sample z. Since much of the underlying optical scattering theory treats C_{ext}, this proportionality is used to connect theory with experimental measurements of A.

C_{ext} of a GNR is a sum of the absorption and scattering cross-sections C_{abs} and C_{sca}, respectively. In the Rayleigh approximation (particles small compared to the wavelength), each of these will depend upon the polarizability tensor $\boldsymbol{\alpha}$ of the GNR:[2,3]

$$C_{abs} = k \frac{\text{Im}\left(\mathbf{E}_0^* \cdot \boldsymbol{\alpha}\mathbf{E}_0\right)}{\mathbf{E}_0^* \cdot \mathbf{E}_0}$$

$$C_{sca} = \frac{k^4}{6\pi} \frac{\left(\boldsymbol{\alpha}\mathbf{E}_0^*\right) \cdot \left(\boldsymbol{\alpha}\mathbf{E}_0\right)}{\mathbf{E}_0^* \cdot \mathbf{E}_0}$$

(S10)

where k is the wavenumber, and $\mathbf{E}_0$ is the incident electric field. For GNRs of the aspect ratios and sizes in our experiments, both absorption and scattering may be significant, so both are included in this analysis.

If we define the long axis of the GNR as "1" and the two transverse axes as "2" (since they are degenerate), the polarizability tensor, in the frame of the GNR, can be written simply as:

$$\boldsymbol{\alpha}_{GNR} = \begin{pmatrix} \alpha_1 & 0 & 0 \\ 0 & \alpha_2 & 0 \\ 0 & 0 & \alpha_2 \end{pmatrix}, \tag{S11}$$

where α_1 is dominant at the LSPR wavelength and α_2 is dominant at the TSPR wavelength.

When a GNR is aligned with its long axis exactly parallel or perpendicular to the polarization of the incident light, the extinction coefficients $C_{ext,1}$ and $C_{ext,2}$ can be obtained from Equations S10, S11:

$$C_{ext,1} = k\,\mathrm{Im}(\alpha_1) + \frac{k^4}{6\pi}|\alpha_1|^2$$
$$C_{ext,2} = k\,\mathrm{Im}(\alpha_2) + \frac{k^4}{6\pi}|\alpha_2|^2 \tag{S12}$$

In experiments in this work, the MagGNR orientations are described by the polar angle θ and azimuthal angle ϕ relative to a magnetic field in the laboratory frame along the x-axis according to the figure above. To predict the optical response for such an arbitrary orientation, one must first write the GNR polarizability in the laboratory frame by appropriate rotation operations:

$$\boldsymbol{\alpha}_{lab}(\theta,\phi) = \mathbf{R}^{-1}(\theta,\phi)\,\boldsymbol{\alpha}_{GNR}\mathbf{R}(\theta,\phi), \tag{S13}$$

where

$$\mathbf{R}(\theta,\phi) = \begin{pmatrix} \cos\theta & \sin\theta\cos\phi & \sin\theta\sin\phi \\ -\sin\theta & \cos\theta\cos\phi & \cos\theta\sin\phi \\ 0 & -\sin\phi & \cos\phi \end{pmatrix}. \tag{S14}$$

Then, to predict the extinction coefficients for an electromagnetic field polarized along x (parallel to $\mathbf{H}$) or y (perpendicular to $\mathbf{H}$), we find $C_{ext,\parallel}$ and $C_{ext,\perp}$, after much simplification, as:

$$C_{ext,\parallel}(\theta) = C_{ext,1}\cos^2\theta + C_{ext,2}\sin^2\theta$$
$$C_{ext,\perp}(\theta,\phi) = C_{ext,1}\sin^2\theta\cos^2\phi + C_{ext,2}\left(\cos^2\theta\cos^2\phi + \sin^2\phi\right) \tag{S15}$$

In this study, measurements of A were analyzed at the LSPR wavelength, in which case $\alpha_2 \ll \alpha_1$ and $C_{ext,2} \ll C_{ext,1}$. We obtain the simplification:

$$C_{ext,\parallel}(\theta) = C_{ext,1}\cos^2\theta$$
$$C_{ext,\perp}(\theta,\phi) = C_{ext,1}\cos^2\phi\sin^2\theta \tag{S16}$$

The measurements are collected over an ensemble of MagGNRs with an angular distribution f_θ, as in Equation 5, which is independent of ϕ. We may assume the MagGNRs have identical optical properties, so that the ensemble averages simplify as follows:

$$A_\parallel \propto \left\langle C_{ext,\parallel}(\theta) \right\rangle = C_{ext,1} \left\langle \cos^2 \theta \right\rangle$$

$$A_\perp \propto \left\langle C_{ext,\perp}(\theta,\phi) \right\rangle = C_{ext,1} \left\langle \cos^2 \phi \sin^2 \theta \right\rangle = \frac{1}{2} C_{ext,1} \left\langle \sin^2 \theta \right\rangle \tag{S17}$$

where both extinctions have the same constants of proportionality (determined by experimental conditions). Therefore, ratiometric parameters can be computed, such as the optical anisotropy:

$$\frac{A_\parallel}{A_\perp} = \frac{C_{ext,1} \left\langle \cos^2 \theta \right\rangle}{C_{ext,1} \left\langle \sin^2 \theta \cos^2 \phi \right\rangle} = 2 \frac{\left\langle \cos^2 \theta \right\rangle}{\left\langle \sin^2 \theta \right\rangle} \tag{S18}$$

and the 3D order parameter:

$$\begin{aligned} S_{3D,optical} &= \frac{A_\parallel - A_\perp}{A_\parallel + 2A_\perp} = \frac{C_{ext,1} \left\langle \cos^2 \theta \right\rangle - C_{ext,1} \left\langle \sin^2 \theta \right\rangle / 2}{C_{ext,1} \left\langle \cos^2 \theta \right\rangle + C_{ext,1} \left\langle \sin^2 \theta \right\rangle} \\ &= \left\langle \cos^2 \theta \right\rangle - \frac{1}{2} \left\langle 1 - \cos^2 \theta \right\rangle \\ &= \frac{3 \left\langle \cos^2 \theta \right\rangle - 1}{2} \end{aligned} \tag{S19}$$

Summary of Analysis of Alignment of MagGNRs

First, we express the 2D order parameter, $S_{2D} = 2 \left\langle \cos^2 \chi \right\rangle - 1$, in terms of the angles θ and ϕ defined in the above figure, so that it can be computed from knowledge of the 3D angular distribution. In this picture, the unit vector corresponding to the long axis of the MagGNR written in the laboratory frame is given by a rotation according to the inverse of the matrix **R** in Equation S14. (Note that the inverse of **R** is also its transpose.) This unit vector is thus:

$$\hat{g} = \mathbf{R}^{-1} \begin{pmatrix} 1 \\ 0 \\ 0 \end{pmatrix} = \hat{i} \cos\theta + \hat{j} \sin\theta \cos\phi + \hat{k} \sin\theta \sin\phi, \tag{S20}$$

and thus,

$$\cos^2 \chi = \frac{g_x^2}{g_x^2 + g_y^2} = \frac{\cos^2 \theta}{\cos^2 \theta + \sin^2 \theta \cos^2 \phi}. \tag{S21}$$

Therefore, the ensemble average is:

$$\left\langle \cos^2 \chi \right\rangle = \int\limits_{0}^{2\pi} \int\limits_{-\pi/2}^{\pi/2} \frac{\cos^2 \theta'}{\cos^2 \theta' + \sin^2 \theta' \cos^2 \phi'} f_{\theta'}(n) \left| \sin \theta' \right| d\theta' d\phi'$$

$$= 2\pi \int\limits_{-\pi/2}^{\pi/2} \cos \theta' f_{\theta'}(n) \left| \sin \theta' \right| d\theta' \qquad , \qquad \text{(S22)}$$

$$= \left\langle \cos \theta \right\rangle$$

and

$$S_{2D} = 2\left\langle \cos^2 \chi \right\rangle - 1 \qquad . \qquad \text{(S23)}$$
$$= 2\left\langle \cos \theta \right\rangle - 1$$

Now that we have expressions for the order parameters S_{2D} and S_{3D} in terms of ensemble averages over functions of θ, we can follow the method as in Equations 5-7 to compute their values for a known trap depth parameter n. Briefly summarized, this would be done by:

$$Z(n) = 2\pi \int\limits_{-\pi/2}^{\pi/2} e^{n \cos^2 \theta'} \left| \sin \theta' \right| d\theta'$$

$$f_\theta(n) = \frac{e^{n \cos^2 \theta}}{Z(n)}$$

$$\left\langle \cos \theta \right\rangle = 2\pi \int\limits_{-\pi/2}^{\pi/2} \cos \theta' f_{\theta'}(n) \left| \sin \theta' \right| d\theta' \qquad , \qquad \text{(S24)}$$

$$\left\langle \cos^2 \theta \right\rangle = 2\pi \int\limits_{-\pi/2}^{\pi/2} \cos^2 \theta' f_{\theta'}(n) \left| \sin \theta' \right| d\theta'$$

$$S_{2D} = 2\left\langle \cos \theta \right\rangle - 1$$

$$S_{3D} = \frac{3\left\langle \cos^2 \theta \right\rangle - 1}{2}$$

where the integrals are evaluated numerically in *Mathematica*.

Synthesis of Small Fe₃O₄ NPs

Oleylamine-stabilized magnetite (Fe_3O_4) NPs with average diameters of 6.6 nm were synthesized by a reductive thermal decomposition method.[4] 1.05 g of iron(III) acetylacetonate was dissolved in a mixture of 15 mL benzyl ether and 15 mL oleylamine, which served as a ligand and reducing agent, in a round-bottomed flask connected to a Schlenk line. The mixture was degassed at room temperature under vacuum for 1 hour, followed by backfilling with nitrogen and heating to 120 °C for another hour under inert atmosphere. The temperature was then quickly increased to 210 °C and held for 1 hour. After allowing the product to cool to room temperature, 50 mL of ethanol was added to assist flocculation of the NPs during centrifugation (Thermo Scientific Sorvall Legend X1R with Fiberlite F15-6x100y rotor) at 4000 rpm (1753 g) for 5 min. The sedimented oleylamine-stabilized Fe_3O_4 NPs were then redispersed in 10 mL chloroform. An aliquot of 0.25 mL from this stock solution was diluted with chloroform to a total volume of 10 mL. PEI functionalization was performed as described in the main text, by adding a solution of 100 mg of PEI dissolved in 30 mL of chloroform with vigorous stirring.

References:
[1]   P. V. Ruijgrok, N. R. Verhart, P. Zijlstra, A. L. Tchebotareva, M. Orrit, *Phys. Rev. Lett.* **2011**, *107*, 037401.
[2]   C. F. Bohren, D. R. Huffman, *Absorption and Scattering of Light by Small Particles*, Wiley, Weinheim, Germany **2004**.
[3]   V. A. Markel, *J. Quant. Spectrosc. Radiat. Transf.* **2019**, *236*, 106611.
[4]   Z. Xu, C. Shen, Y. Hou, H. Gao, S. Sun, *Chem. Mater.* **2009**, *21*, 1778.
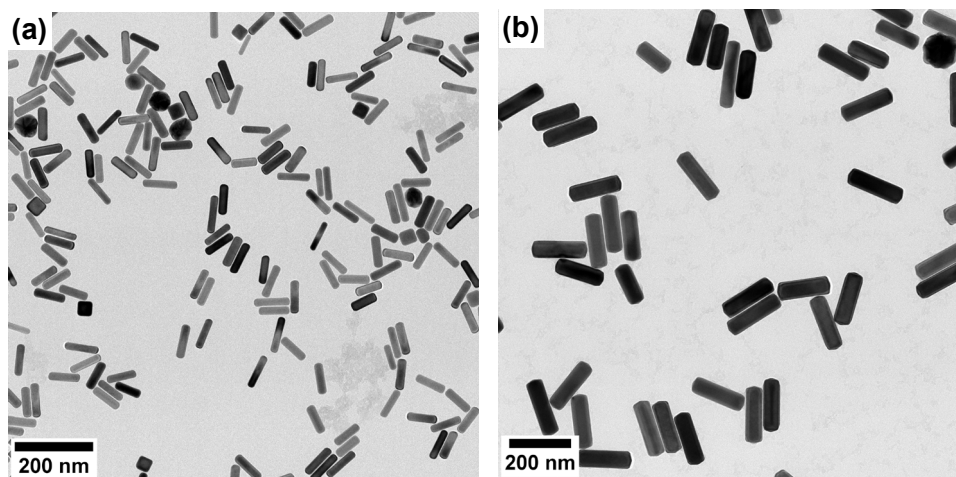
Figure S1. TEM images of (a) small and (b) large BSA-GNRs.
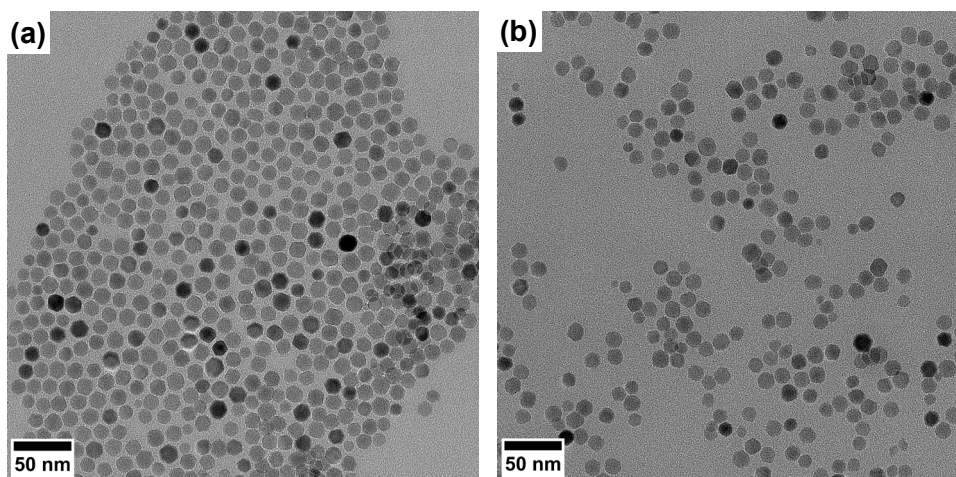
Figure S2. TEM images of Fe$_3$O$_4$ NPs (a) stabilized with native oleic acid ligands and (b) after functionalization with PEI.
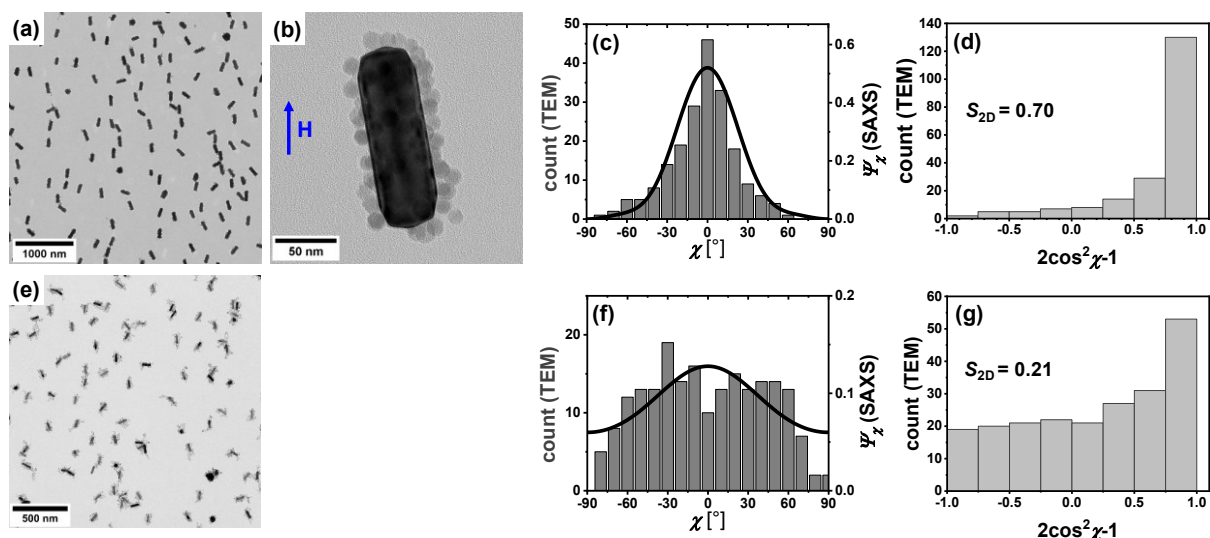
Figure S3. TEM images of large MagGNRs dried under 10 kOe magnetic field parallel to the grid and in the vertical direction in the images at (a) lower magnification (b) higher magnification. (c) Angular distribution overlaid with the corresponding distributions from SAXS measurements and (d) S_{2D} calculated from measurements of 200 aligned large MagGNRs. The same (e) imaging in 10 kOe field, (f) measurements and tabulation of the angular distribution, and (g) calculation of S_{2D} were performed on 200 aligned small MagGNRs.
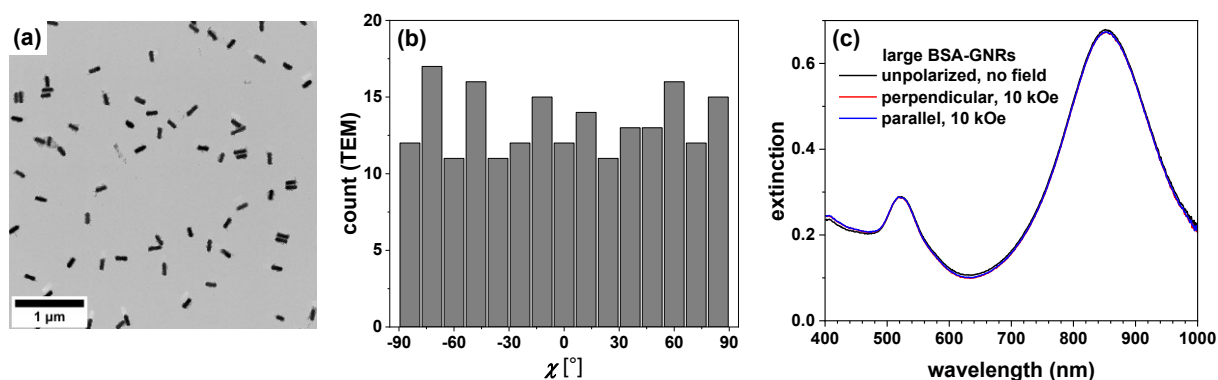
Figure S4. Control experiments confirming no alignment without combined use of magnetic overcoatings and magnetic fields. (a) Large MagGNRs dried without a magnetic field and imaged by TEM with (b) measurements of the angular distribution of 200 MagGNRs with respect to the vertical direction. (c) Unpolarized and polarized optical extinction spectra of BSA-GNRs measured in 10 kOe field in an electromagnet.
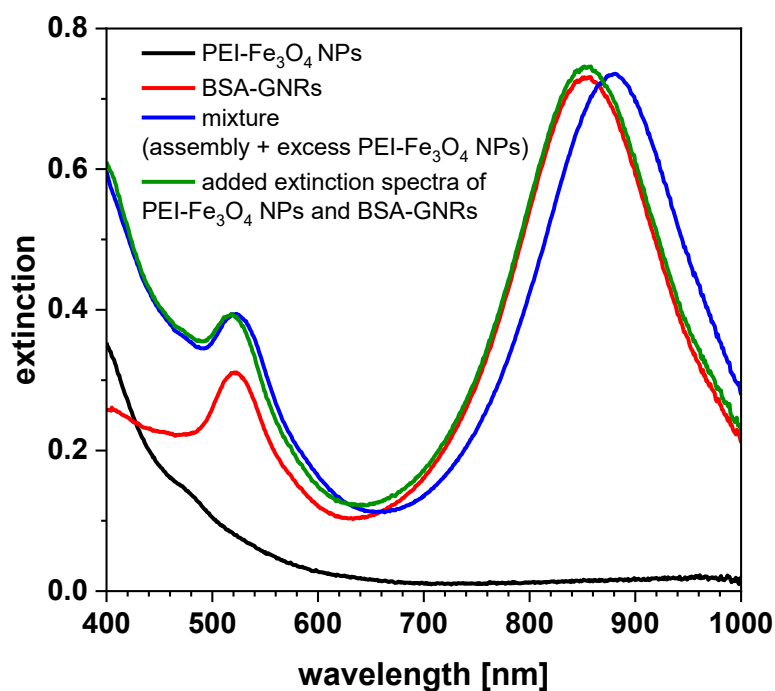
Figure S5. The extinction of the GNR core is preserved after assembly of MagGNRs. Extinction spectra of large BSA-GNRs and PEI-Fe₃O₄ NPs before and after mixing for two hours and before purification are compared with their sum. The spectra have been adjusted to account for dilution effects. The mixture contains MagGNRs and excess PEI-Fe₃O₄ NPs. The LSPR intensity is not affected in the MagGNRs, and a redshift is observed, which is discussed in the main text. The consistent intensity of the LSPR during assembly validates normalization of the extinction spectra of BSA-GNRs and MagGNRs at the LSPR in Figure 3.
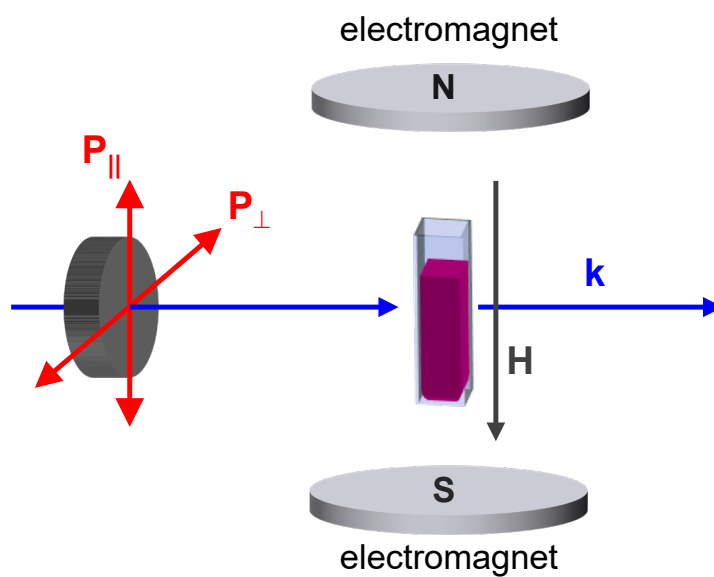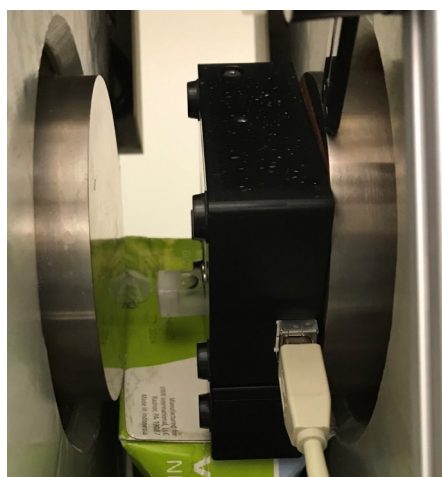
Figure S6. (Left) Photograph of the spectrophotometer placed between the poles of the electromagnet and (right) schematic (rotated 90° clockwise with respect to the photograph) of spectroscopy measurements in the electromagnet, with light of polarization **P** propagating along **k**.
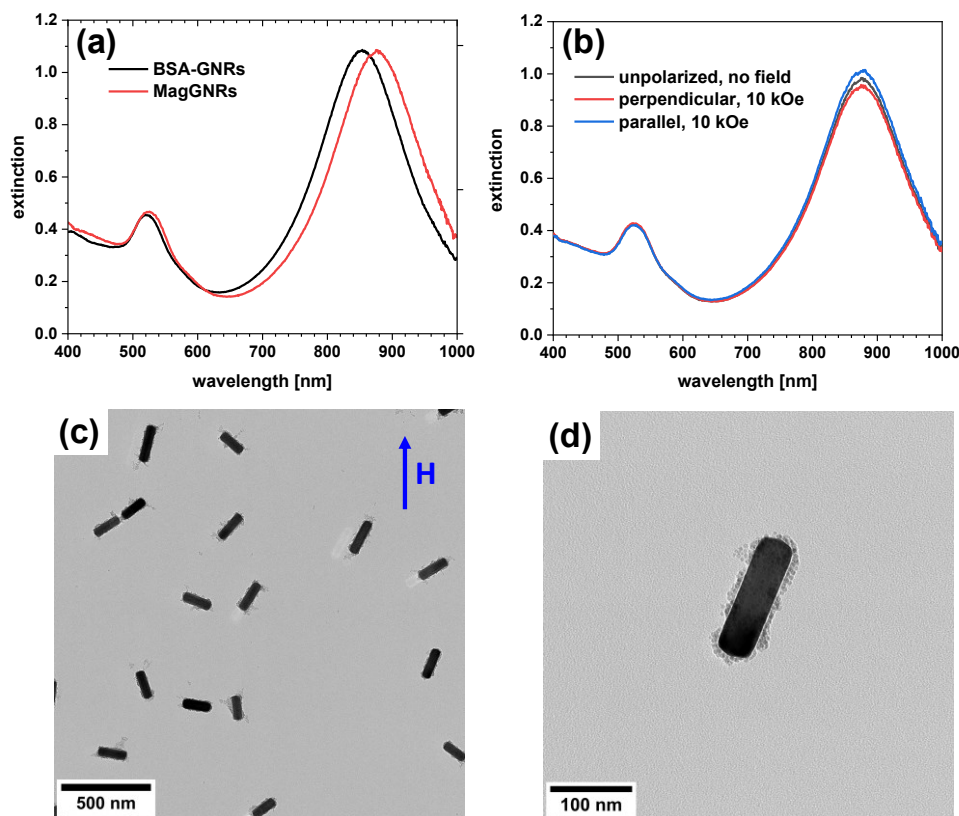
Figure S7. (a) Extinction spectra of large BSA-GNRs and MagGNRs prepared with small, 6.6 nm PEI-Fe$_3$O$_4$ NPs. (b) Polarized extinction spectra of these MagGNRs in a 10 kOe magnetic field. TEM images (c) after drying in a 10 kOe magnetic field, including (d) a magnified image of a single MagGNR.
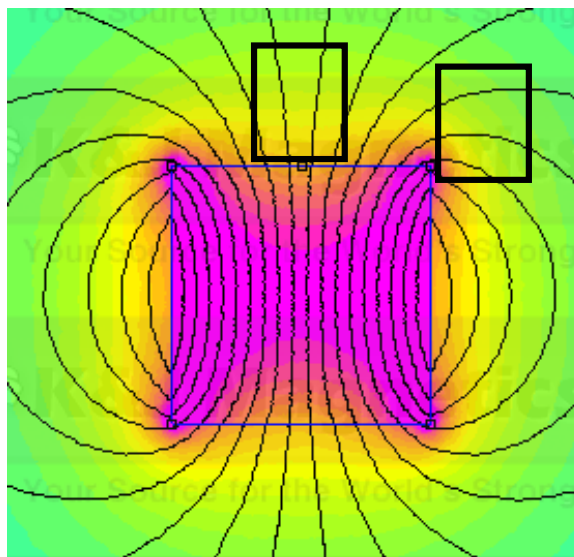
Figure S8. Magnetic field distribution around 1 in. N52 cube magnet, calculated using https://www.kjmagnetics.com/calculator.asp. Approximate locations of the cuvettes with MagGNRs in Figure 5a-c are indicated by overlaid rectangles.
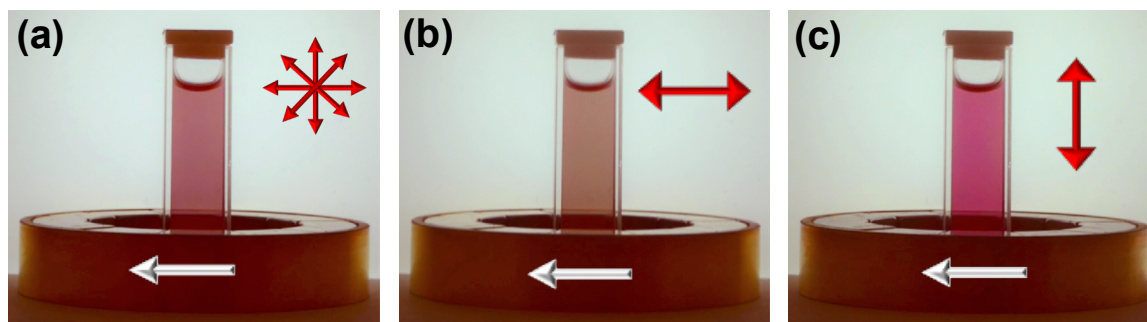
Figure S9. Photos of large MagGNRs in a horizontal magnetic field generated by a circular Halbach array (a) unpolarized and with (b) horizontal and (c) vertical polarizer films. The magnetic field and polarizer directions are indicated by single-headed and double-headed arrows, respectively.
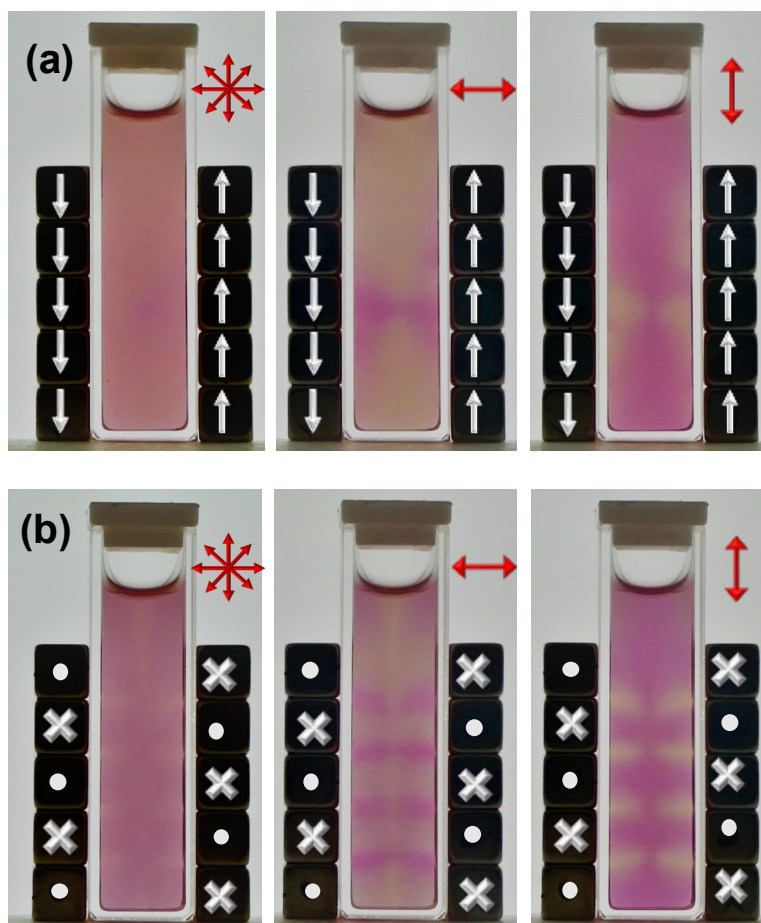
Figure S10. Photos of cuvette with large MagGNRs placed between arrays of five ¼ in. cube magnets without and with polarizer for (a) vertical, in-plane and (b) out-of-plane magnetic fields.
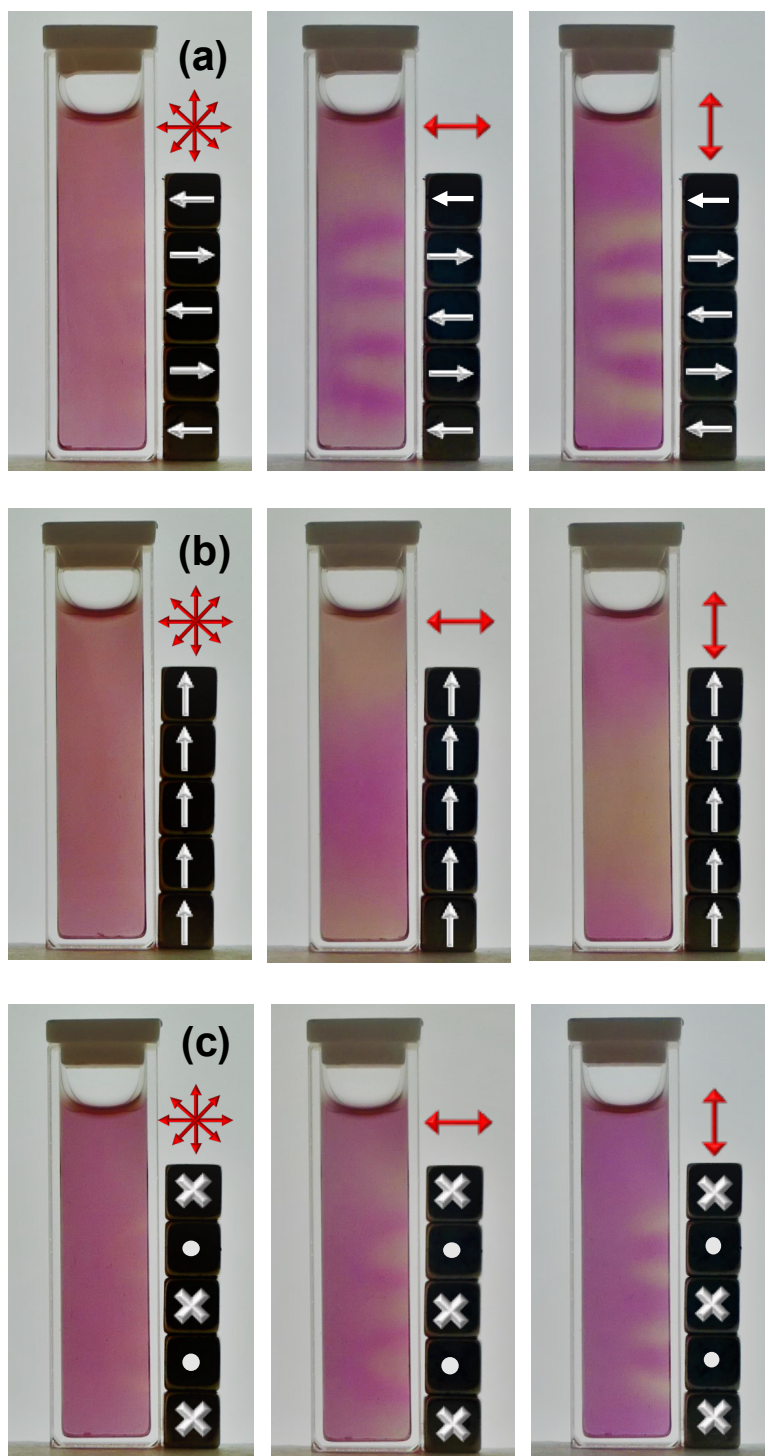
Figure S11. Photos of cuvette with large MagGNRs placed next to a single array of five ¼ in. cube magnets without and with polarizer for (a) horizontal, in-plane, (b) vertical, in-plane, and (c) out-of-plane magnetic fields.
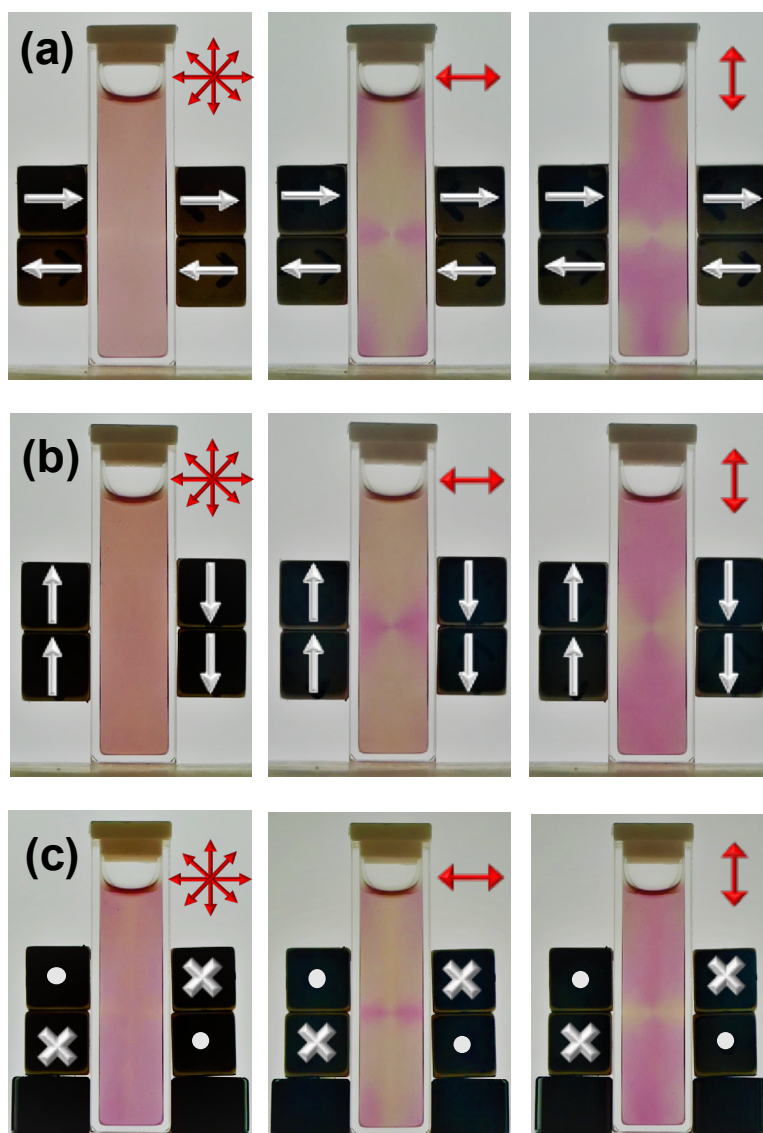
Figure S12. Photos of cuvette with large MagGNRs placed between arrays of two 10 mm cube magnets without and with polarizer for (a) horizontal, in-plane, (b) vertical, in-plane, and (c) out-of-plane magnetic fields.
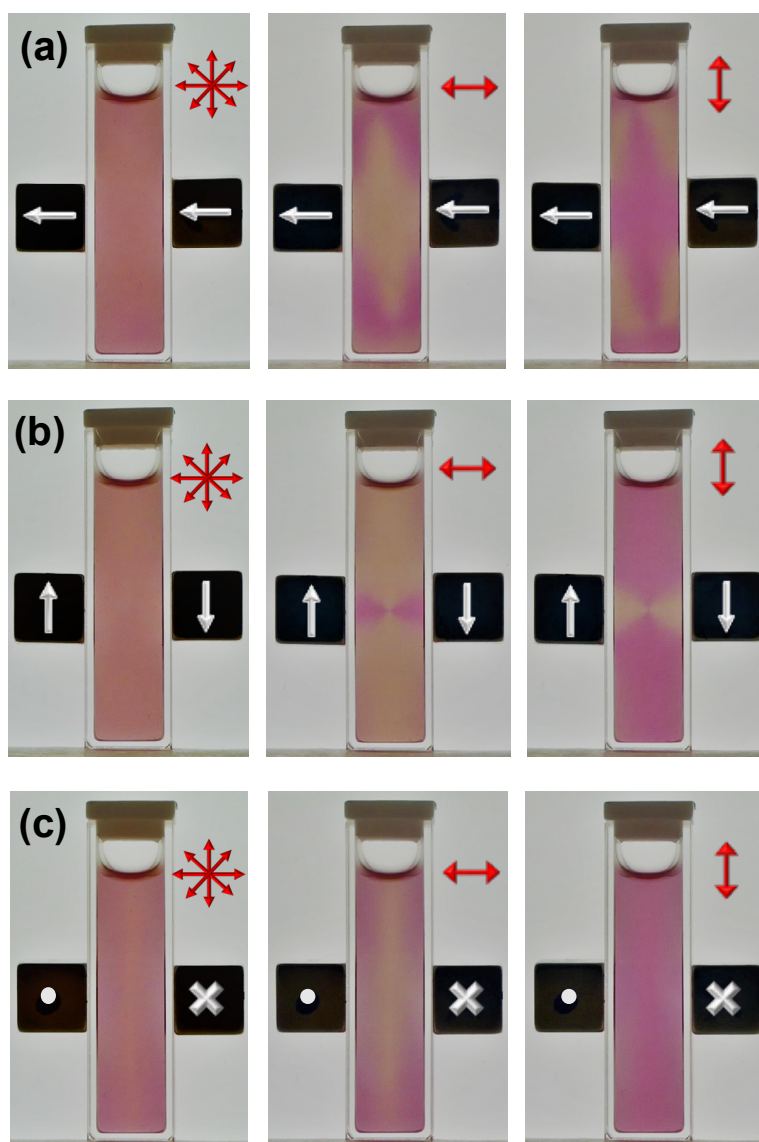
Figure S13. Photos of cuvette with large MagGNRs placed between a pair of 10 mm cube magnets without and with polarizer for (a) horizontal, in-plane, (b) vertical, in-plane, and (c) out-of-plane magnetic fields.
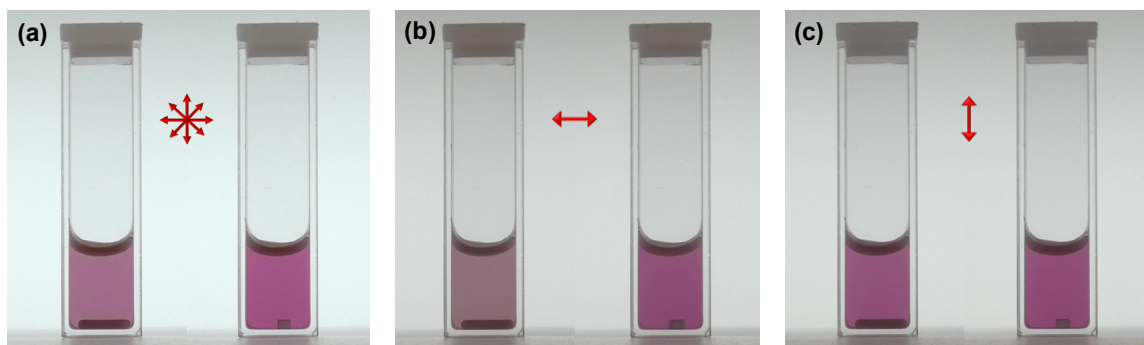
Figure S14. Pairs of snapshots from Movie S8 of large MagGNRs with a stir bar placed on a stir plate with the field (left photo) in-plane or (right photo) out-of-plane (a) without a polarizer, (b) with a horizontal polarizer, and (c) with a vertical polarizer.
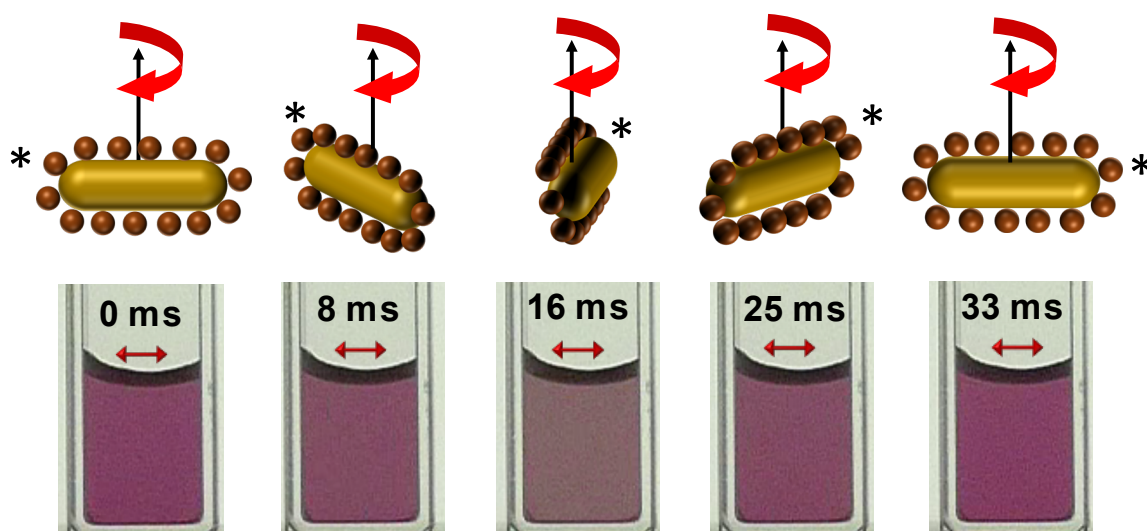

Figure S15. Snapshots from Movie S9 of large MagGNRs rotating on a stir plate set at 1000 rpm with a horizontal polarizer. Analysis of the video shows that 120 cycles of color change, corresponding to 60 full rotations, occur in 3.634 s, which is equivalent to a speed of 991 rpm.
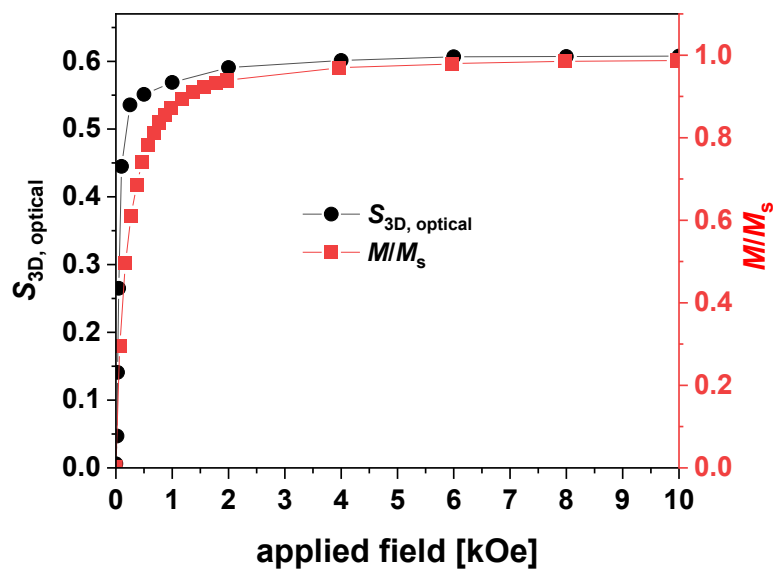
Figure S16. $S_{3D, optical}$ and magnetization of MagGNRs as a function of applied magnetic field.